

ADAPTIVITY IN SPACE AND TIME FOR MAGNETOQUASISTATICS*

Markus Clemens

Helmut-Schmidt-Universität Hamburg, Holstenhofweg 85, 22043 Hamburg, Germany
Email: m.clemens@hsu-hh.de

Jens Lang

Technische Universität Darmstadt, Schlossgartenstraße 7, 64289 Darmstadt, Germany
Email: lang@mathematik.tu-darmstadt.de

Delia Teleaga

Technische Universität Darmstadt, Schlossgartenstraße 7, 64289 Darmstadt, Germany
Email: dteleaga@mathematik.tu-darmstadt.de

Georg Wimmer

Helmut-Schmidt-Universität Hamburg, Holstenhofweg 85, 22043 Hamburg, Germany
Email: g.wimmer@hsu-hh.de

Abstract

This paper addresses fully space-time adaptive magnetic field computations. We describe an adaptive Whitney finite element method for solving the magnetoquasistatic formulation of Maxwell's equations on unstructured 3D tetrahedral grids. Spatial mesh refinement and coarsening are based on hierarchical error estimators especially designed for combining tetrahedral $\mathbf{H}(\mathbf{curl})$ -conforming edge elements in space with linearly implicit Rosenbrock methods in time. An embedding technique is applied to get efficiency in time through variable time steps. Finally, we present numerical results for the magnetic recording write head benchmark problem proposed by the Storage Research Consortium in Japan.

Mathematics subject classification: 65M60, 65L06, 78M10

Key words: Magnetoquasistatics, Space-time adaptivity, Edge elements, Rosenbrock methods, Hierarchical error estimator, SRC benchmark problem.

1. Introduction

The magnetoquasistatic approximation (MQS) arises from Maxwell's equations by dropping the displacement current. This is reasonable for many electrical machines, generators and transformers which work in the low-frequency high-conductivity range. Wave propagation can then be neglected and vanishing tangential traces are used for artificial boundary conditions [18].

In this work we develop a fully adaptive algorithm to solve general three-dimensional non-linear MQS problems. The local accuracy of the numerical solution is controlled by means of a posteriori error estimates in space and time. In the past, computational electromagnetics has mainly focused on efficiency by (i) applying advanced multigrid algorithm with optimal complexity to solve large scale linear systems, e.g., [11, 17, 19, 28, 34], (ii) adapting spatial grids by means of a posteriori error estimators [8, 12, 32, 37], and to some extent by (iii) optimizing time grids in accordance with local error control [13, 15, 16, 40]. An interesting alternative approach is the goal-oriented weighted dual method [10]. Often, in addition, highly parallelized strategies

* Received November 30, 2007 / Revised version received June 26, 2008 / Accepted February 5, 2009 /

are applied. On the other side the reliability question, that is, how accurate is the numerical solution computed, has received much less attention in MQS simulation.

There is nowadays an increasing emphasis on all aspects of adaptively generating a space-time grid that evolves with the solution. Equally important is the development of efficient higher-order one-step integration methods which can handle very stiff differential-algebraic electromagnetic problems and which allow us to accommodate a grid in each time step without any specific difficulties. Combined space-time adaptivity is widely used in computational fluid dynamics and thermodynamics, see, e.g., [39].

Recently, first investigations for space and time adaptive MQS solvers have been made in [42] where first-order approximations in time and space are considered and in [41] where higher-order embedded SDIRK-methods are used for first-order spatial discretizations. In [31] a new variable step-size one-step Rosenbrock methods ROS3PL is coupled with lowest-order edge elements to solve linear MQS problems. Here, we extend the latter approach to nonlinear material laws. We wish to adaptively refine space-time grids in order to capture local effects efficiently and reliably in accordance to imposed temporal and spatial tolerances. We apply the adaptive Rothe method based on the discretization sequence first in time then in space, in contrast to the usual Method of Lines approach (see, e.g., [29] and references therein). The spatial discretization is considered as a perturbation of the time integration process. Implementations have been done in the KARDOS library [2, 23], which provides a suitable programming environment for adaptive algorithms to solve nonlinear time-dependent PDEs.

2. Problem Class

Introducing a vector potential $\mathbf{A}(\mathbf{x}, t)$ for the magnetic induction $\mathbf{B} = \nabla \times \mathbf{A}$, we consider the equations of magnetoquasistatics for isotropic materials in the form

$$\begin{aligned} \sigma \partial_t \mathbf{A} + \nabla \times (\mu^{-1}(|\nabla \times \mathbf{A}|) \nabla \times \mathbf{A}) &= \mathbf{J}_s, \quad \text{in } \Omega \times (0, T], \\ \mathbf{A} \times \mathbf{n} &= \mathbf{0}, \quad \text{on } \partial\Omega \times (0, T], \\ \mathbf{A}(\cdot, 0) &= \mathbf{A}_0, \quad \text{on } \Omega \end{aligned} \quad (2.1)$$

where σ is the scalar electric conductivity and $\mathbf{J}_s(\mathbf{x}, t)$ denotes the applied current density which has to satisfy the consistency condition $\nabla \cdot \mathbf{J}_s = 0$. The scalar magnetic permeability μ is in general nonlinear and is defined by the material relation $\mathbf{H} = \mu^{-1}(|\mathbf{B}|)\mathbf{B}$ between the magnetic field \mathbf{H} and the magnetic induction \mathbf{B} . Here, $|\cdot|$ stands for the usual Euclidean vector norm. Due to physical arguments, the continuous function $\mu^{-1}(s) : \mathbb{R}_0^+ \rightarrow \mathbb{R}^+$ satisfies the following properties [35]:

$$\begin{aligned} 0 < \underline{\mu}^{-1} \leq \mu^{-1}(s) \leq \mu_0^{-1} \quad \text{for all } s, \\ f(s) = s\mu^{-1}(s) \quad \text{is strictly monotone and Lipschitz continuous,} \end{aligned} \quad (2.2)$$

where $\mu_0 = 4\pi \times 10^{-7} \text{Hm}^{-1}$ is the permeability in vacuum.

Since there may be insulating regions with $\sigma = 0$, system (2.1) is in general an elliptic-parabolic initial-boundary value problem. The physically relevant quantities which can be derived from \mathbf{A} are the magnetic induction $\mathbf{B} = \nabla \times \mathbf{A}$ and the eddy current density $\mathbf{J}_E = -\sigma \partial_t \mathbf{A}$. The vector potential formulation (2.1) is widely used in electromagnetic computations since it has no problems with multiple connected conductive domains. However, there are two essential difficulties: the uniqueness of \mathbf{A} in parts of the domain where $\sigma = 0$, and the

consistency of \mathbf{J}_s which has to be ensured on each spatial mesh. A detailed discussion of the latter can be found in [36]. For gauging, we use a (small) positive conductivity $\sigma_\varepsilon = \varepsilon > 0$ in the non-conducting regions. A rigorous justification of this regularization is given in [5]. Using a strictly positive conductivity in the whole computational domain Ω , unique solvability of the slightly perturbed problem (2.1) in the space $\mathbf{H}_0(\mathbf{curl})$ can be assumed.

3. Linearly Implicit Methods in Time

To approximate the vector potential $\mathbf{A}(\cdot, t)$ defined in (2.1) by values $\mathbf{A}_n \approx \mathbf{A}(\cdot, t_n)$ at a certain time grid

$$0 = t_0 < t_1 < \dots < t_n < \dots < t_{M-1} < t_M = T, \tag{3.1}$$

we apply an s -stage linearly implicit one-step method of Rosenbrock type (see [26], formula IV.7(7.27), or [29], formula V.1(V.12)). This has the form

$$\mathbf{A}_{n+1} = \mathbf{A}_n + \sum_{i=1}^s m_i \mathbf{A}_{ni}, \tag{3.2}$$

with stage values \mathbf{A}_{ni} , $i = 1, \dots, s$, determined from the linear equations

$$\begin{aligned} \nabla \times (\mathbf{T}_n \nabla \times \mathbf{A}_{ni}) + \frac{\sigma}{\tau_n \gamma} \mathbf{A}_{ni} &= \mathbf{R}_{ni}, & \text{in } \Omega, \\ \mathbf{A}_{ni} \times \mathbf{n} &= 0, & \text{on } \partial\Omega, \end{aligned} \tag{3.3}$$

with the time step $\tau_n = t_{n+1} - t_n$ and γ being the stability constant of the method. The symmetric matrix \mathbf{T}_n is derived from a linearization of the nonlinear operator $\nabla \times (\mu^{-1}(|\nabla \times \mathbf{A}|)\nabla \times \mathbf{A})$ with respect to \mathbf{A} at time t_n

$$\mathbf{T}_n = \mu^{-1}(|\nabla \times \mathbf{A}_n|) \mathbf{I} + (\mu^{-1})'(|\nabla \times \mathbf{A}|)_{|\mathbf{A}=\mathbf{A}_n} \frac{(\nabla \times \mathbf{A}_n)(\nabla \times \mathbf{A}_n)^T}{|\nabla \times \mathbf{A}_n|}. \tag{3.4}$$

Here, \mathbf{I} denotes the 3×3 -identity matrix and $(\nabla \times \mathbf{A}_n)(\nabla \times \mathbf{A}_n)^T$ is a 3×3 -matrix of rank 1. Asymptotic analysis shows $\mathbf{T}_n \rightarrow \mu^{-1}(0) \mathbf{I}$ for $|\nabla \times \mathbf{A}_n| \rightarrow 0$ [6]. The right hand side \mathbf{R}_{ni} in (3.3) is defined by

$$\begin{aligned} \mathbf{R}_{ni} &= -\nabla \times (\mu^{-1}(|\nabla \times \mathbf{A}_i|) \nabla \times \mathbf{A}_i) + \mathbf{J}_s(\cdot, t_i) \\ &\quad - \sigma \sum_{j=1}^{i-1} \frac{c_{ij}}{\tau_n} \mathbf{A}_{nj} + \tau_n \gamma_i \partial_t \mathbf{J}_s(\cdot, t_n), \end{aligned} \tag{3.5}$$

where

$$\mathbf{A}_i = \mathbf{A}_n + \sum_{j=1}^{i-1} a_{ij} \mathbf{A}_{nj} \quad \text{and} \quad t_i = t_n + \alpha_i \tau_n.$$

Observe that the system (3.3) has to be solved successively for $i = 1, \dots, s$. Since \mathbf{T}_n does not depend on the stage number i , the stiffness matrix of the linear systems has to be computed only once for all stage values. It is the fundamental idea of Rosenbrock methods that an iterative Newton method as known from implicit Runge-Kutta methods is no longer required. In addition, the stage values \mathbf{A}_{ni} can be also used to derive approximations $\mathbf{Z}_n \approx \partial_t \mathbf{A}(\cdot, t_n)$

of the same order to the first derivative and therefore for the eddy current density \mathbf{J}_E . We compute

$$\mathbf{Z}_{n+1} = \mathbf{Z}_n + \sum_{i=1}^s m_i \left(\frac{1}{\tau_n} \sum_{j=1}^i (c_{ij} - s_{ij}) \mathbf{A}_{nj} + (d_i - 1) \mathbf{A}_n \right). \tag{3.6}$$

The stage number s and the defining formula coefficients $m_i, c_{ij}, \gamma_i, a_{ij}, d_i, s_{ij}, \alpha_i$, and γ are chosen to obtain a desired order of consistency and good stability properties for differential-algebraic equations [29].

The A-stable Rosenbrock solver ROS3P from [30] was constructed for parabolic problems. For differential-algebraic equations (as (2.1) with $\sigma = 0$ somewhere in computational domain), we would like to have also L-stability and the property of stiff accuracy [26]. Clearly, these new features are also valuable for singular perturbed problems, that is when a small σ is used in the insulation region. The arising system is then very stiff and behaves like a differential-algebraic equation. For this, we have designed a new third-order Rosenbrock solver ROS3PL. Special care has to be taken to avoid order reduction - a phenomenon which is not induced by lack of smoothness of the solution but rather by the presence of powers of differential operators in the local truncation error. Fortunately, there are conditions which imply also higher order of convergence (see [29] and [30] for more details). In practical problems, the nonlinear function $\mu^{-1}(|\nabla \times \mathbf{A}|)$ is given by a set of measured data points which has to be interpolated to obtain a continuous $\mathbf{B}\text{-}\mathbf{H}$ -curve. In consequence, only an approximation of the derivative $(\mu^{-1})'(|\nabla \times \mathbf{A}|)_{|\mathbf{A}=\mathbf{A}_n}$ is available to compute \mathbf{T}_n from (3.4). Thus, it is worth satisfying additional conditions, that is conditions for W-methods, to be more robust with respect to perturbed Jacobians. The original idea of W-methods is to ensure the classical order for Rosenbrock methods for all approximations of the Jacobian ([26], section IV.7, p. 114). Here, we ensure third-order accuracy for approximations of the form $\hat{\mathbf{T}}_n = \mathbf{T}_n + \mathcal{O}(\tau_n)$. It turns out that such a method exists with $s=4$ and three function evaluations only. The set of coefficients for ROS3PL is given in Tab. A1 in the appendix.

Rosenbrock methods offer a simple way to estimate the local error. A second solution $\hat{\mathbf{A}}_{n+1}$ of inferior order, say \hat{p} , can be computed by replacing the original weights m_i by \hat{m}_i in (3.2). In order to take into account the scale of the problem, the local error estimator is defined by the weighted root mean square norm

$$r_{n+1} = \left(\frac{\|\mathbf{A}_{n+1} - \hat{\mathbf{A}}_{n+1}\|_{L^2(\Omega)}^2}{ATOL + RTOL \|\mathbf{A}_{n+1}\|_{L^2(\Omega)}^2} \right)^{1/2}. \tag{3.7}$$

The tolerances $ATOL$ and $RTOL$ have to be selected carefully to furnish meaningful input for the error control. The estimator can be used to propose a new time step by

$$\tau_{n+1} = \frac{\tau_n}{\tau_{n-1}} \left(\frac{TOL_t r_n}{r_{n+1} r_{n+1}} \right)^{1/(\hat{p}+1)} \tau_n, \tag{3.8}$$

where TOL_t is a desired tolerance prescribed by the user [25]. If $r_{n+1} > TOL_t$ the step is rejected and redone. Otherwise the step is accepted and we advance in time. The order of the embedded solution of ROS3PL is $\hat{p}=2$. Rosenbrock methods have been successfully applied to linear and to nonlinear magnetic field problems [16,31].

4. Multilevel Edge Elements in Space

We employ a multilevel finite element method based on Nédélec’s curl-conforming ansatz functions [4, 33] to solve the s linear systems (3.3) in each time step. This enforces the typical tangential continuity of the vector potential \mathbf{A}_n across interelement boundaries. Families of shape-regular tetrahedral meshes are generated by repeated refinement of initial triangulations \mathcal{T}_{n+1}^0 at t_{n+1} , $n = 0, \dots, M - 1$. So, the solution space is replaced by sequences of discrete spaces with successively increasing dimension to improve their approximation property. After a successful time step we coarsen the mesh in regions where degrees of freedom are no longer needed. To steer local refinement and coarsening, we compute a posteriori error estimates based on a hierarchical decomposition. Further, the information about the global accuracy of the finite element solution is also used to balance the spatial and temporal errors during our adaptive time stepping procedure.

Adaptive multilevel methods have proven to be a useful tool for drastically reducing the size of the arising linear algebraic systems and to achieve high and controlled accuracy of the spatial discretization [21, 29]. For stationary and time-harmonic Maxwell problems, they have been considered in [6, 7, 9, 38]. In [31], we have extended hierarchical error estimation from [9] to linear MQS approximations. Due to the linearly implicit nature of Rosenbrock methods, this approach can be directly carried over to nonlinear MQS.

Let \mathcal{T}_{n+1}^0 be an admissible initial tetrahedral mesh at time t_{n+1} with a characteristic mesh size $h > 0$ and $\mathcal{N}\mathcal{D}_q^h$ be the associated global $\mathbf{H}_0(\mathbf{curl})$ -conforming space of edge elements of order $q \in \mathbb{N}$. For any tetrahedron T the local spaces are given by

$$\mathcal{N}\mathcal{D}_q(T) = (\Pi_{q-1}(T))^3 + \{ \mathbf{p} \in (\Pi_q(T))^3 : \mathbf{x}^T \mathbf{p}(\mathbf{x}) = 0 \quad \forall \mathbf{x} \in T \} , \tag{4.1}$$

where $\Pi_k(T)$ denotes the space of polynomials of degree at most k over T .

Considering the lowest order case $q = 1$, the Galerkin approximation $\mathbf{A}_{ni}^h \in \mathcal{N}\mathcal{D}_1^h$ of the stage values $\mathbf{A}_{ni} \in \mathbf{H}_0(\mathbf{curl})$, $i = 1, \dots, s$, satisfies the weak formulation

$$b_n(\mathbf{A}_{ni}^h, \mathbf{V}^h) = (\mathbf{R}_{ni}, \mathbf{V}^h) \quad \forall \mathbf{V}^h \in \mathcal{N}\mathcal{D}_1^h, \tag{4.2}$$

where the bilinear form $b_n(\cdot, \cdot)$ is defined as

$$b_n(\mathbf{A}_{ni}^h, \mathbf{V}^h) = (\mathbf{T}_n \nabla \times \mathbf{A}_{ni}^h, \nabla \times \mathbf{V}^h) + \left(\frac{\sigma}{\tau_n \gamma} \mathbf{A}_{ni}^h, \mathbf{V}^h \right)$$

and (\cdot, \cdot) stands for the usual scalar product in $L^2(\Omega)$. A local basis of lowest order edge elements on a tetrahedron T can be explicitly derived from the barycentric coordinate functions λ_i , $i = 1, \dots, 4$, of T [4]:

$$\mathcal{N}\mathcal{D}_1(T) = \text{span}\{ \phi_1, \dots, \phi_6 \}, \quad \phi_k = \lambda_i \nabla \lambda_j - \lambda_j \nabla \lambda_i, \tag{4.3}$$

where ϕ_k is associated with edge k defined by endpoints i and j . We note that the operator associated with the bilinear form $b_n(\cdot, \cdot)$ is independent of the stage level i , and thus the calculation of the corresponding stiffness matrix is required only once within each time step. The linear systems are efficiently solved by an AMG solver with Hiptmair smoother [28] implemented in the package ML of the Trilinos library [27].

After computing approximations \mathbf{A}_{ni}^h to all stage values \mathbf{A}_{ni} from (4.2), a posteriori error estimates for the approximate Rosenbrock solution $\mathbf{A}_{n+1}^h \in \mathcal{N}\mathcal{D}_1^h$ can be used to give specific

assessment of the error distribution and to improve the spatial discretization. We want to estimate the error $\mathbf{A}_{n+1} - \mathbf{A}_{n+1}^h$ caused by the interpolation error of the initial value \mathbf{A}_n and by the spatial approximation to all stage values $\mathbf{A}_{ni} \in \mathbf{H}_0(\mathbf{curl})$, $i = 1, \dots, s$. Here, \mathbf{A}_n has to be understood as error-controlled finite element approximation on the finest mesh \mathcal{T}_n at time t_n .

We define a hierarchical decomposition

$$\mathcal{ND}_2^h = \mathcal{ND}_1^h \oplus \widetilde{\mathcal{ND}}_2^h \quad (4.4)$$

where $\widetilde{\mathcal{ND}}_2^h$ is the surplus space needed to extend the space \mathcal{ND}_1^h to higher order. The idea of a hierarchical error estimator is to bound the spatial error by evaluating its components in the space $\widetilde{\mathcal{ND}}_2^h$ only. For this, we define an a posteriori error estimator $\mathbf{E}_{n+1}^h \in \widetilde{\mathcal{ND}}_2^h$ as

$$\mathbf{E}_{n+1}^h = \mathbf{E}_{n0}^h + \sum_{i=1}^s m_i \mathbf{E}_{ni}^h \quad (4.5)$$

with \mathbf{E}_{n0}^h approximating the projection error of the initial value, i.e., the distance between \mathbf{A}_n taken on the finest mesh \mathcal{T}_n at time t_n and its approximation \mathbf{A}_n^h in \mathcal{ND}_1^h ,

$$b_n(\mathbf{E}_{n0}^h, \Phi) = b_n(\mathbf{A}_n - \mathbf{A}_n^h, \Phi), \quad \forall \Phi \in \widetilde{\mathcal{ND}}_2^h \quad (4.6)$$

and \mathbf{E}_{ni}^h estimating the spatial error of the stage value \mathbf{A}_{ni}^h

$$b_n(\mathbf{E}_{ni}^h, \Phi) = (\mathbf{R}_{ni}^h, \Phi) - b_n(\mathbf{A}_{ni}^h, \Phi), \quad \forall \Phi \in \widetilde{\mathcal{ND}}_2^h \quad (4.7)$$

where

$$\mathbf{R}_{ni}^h = \mathbf{R}_{ni}(\mathbf{A}_{n1}^h + \mathbf{E}_{n1}^h, \dots, \mathbf{A}_{ni-1}^h + \mathbf{E}_{ni-1}^h).$$

Solving (4.6)-(4.7) still encounters a sequence of $s+1$ large linear problems in the space of hierarchical surpluses. From many practical computations, we have experienced that using the approximate error estimator

$$\mathbf{E}_{n+1}^h \approx \tilde{\mathbf{E}}_{n+1}^h = \mathbf{E}_{n0}^h + \frac{1}{\gamma} \mathbf{E}_{n1}^h, \quad (4.8)$$

that is an error estimator for the embedded, locally second order linearly implicit Euler solution

$$\mathbf{A}_{n+1}^{h,euler} = \mathbf{A}_n^h + \mathbf{A}_{n1}^h/\gamma,$$

is quite efficient. This yields the following simplified error equation for $\tilde{\mathbf{E}}_{n+1}^h \in \widetilde{\mathcal{ND}}_2^h$

$$b_n(\tilde{\mathbf{E}}_{n+1}^h, \Phi) = b_n(\mathbf{A}_n - \mathbf{A}_{n+1}^{h,euler}, \Phi) + \frac{1}{\gamma} (\mathbf{R}_{n1}^h, \Phi), \quad \forall \Phi \in \widetilde{\mathcal{ND}}_2^h. \quad (4.9)$$

\mathbf{R}_{n1}^h can be computed from (3.5) as

$$\mathbf{R}_{n1}^h = -\nabla \times \left(\mu^{-1} (|\nabla \times \mathbf{A}_n^h|) \nabla \times \mathbf{A}_n^h \right) + \mathbf{J}_s(\cdot, t_n) + \tau_n \gamma_1 \partial_t \mathbf{J}_s(\cdot, t_n).$$

Although we have reduced the number of error equations considerably, we still face a fully coupled system over the surplus space $\widetilde{\mathcal{ND}}_2^h$ in (4.9). Following the approach given in [9], we

take further advantage of a localization strategy. The idea is to replace the bilinear form $b_n(\cdot, \cdot)$ on the left hand side in (4.9) by a spectrally equivalent preconditioner $c_n(\cdot, \cdot)$ in the surplus space. This is described next.

Defining on each triangle T with barycentric coordinate functions $\lambda_i, i = 1, \dots, 4$, the basis functions

$$\begin{aligned} \tilde{\phi}_{ij} &= \lambda_i \nabla \lambda_j + \lambda_j \nabla \lambda_i, & 1 \leq i < j \leq 4 \\ \tilde{\phi}_{ijk}^{(1)} &= \lambda_k \lambda_i \nabla \lambda_j + \lambda_k \lambda_j \nabla \lambda_i, & 1 \leq i < j < k \leq 4 \\ \tilde{\phi}_{ijk}^{(2)} &= \lambda_k \lambda_i \nabla \lambda_j + \lambda_i \lambda_j \nabla \lambda_k, & 1 \leq i < j < k \leq 4 \end{aligned}$$

a suitable global basis of $\widetilde{\mathcal{ND}}_2^h$ reads as

$$\widetilde{\mathcal{ND}}_2^h = \text{span} \left\{ \tilde{\phi}_e, \tilde{\phi}_f^{(1)}, \tilde{\phi}_f^{(2)} : e = (ij) \text{ edge of } \mathcal{T}_h, f = (ijk) \text{ face of } \mathcal{T}_h \right\}. \tag{4.10}$$

This defines a direct decomposition of the hierarchical surplus space

$$\widetilde{\mathcal{ND}}_2^h = \sum_{\text{edge } e} \widetilde{\mathcal{ND}}_2^h(e) \oplus \sum_{\text{face } f} \widetilde{\mathcal{ND}}_2^h(f) \tag{4.11}$$

with

$$\widetilde{\mathcal{ND}}_2^h(e) = \text{span} \{ \tilde{\phi}_e \} \text{ and } \widetilde{\mathcal{ND}}_2^h(f) = \text{span} \{ \tilde{\phi}_f^{(1)}, \tilde{\phi}_f^{(2)} \}.$$

We note that $\nabla \times \tilde{\phi}_e = 0$ for all edges e . Let

$$\tilde{\mathbf{q}} = \sum_e q_e \tilde{\phi}_e + \sum_f (q_f^{(1)} \tilde{\phi}_f^{(1)} + q_f^{(2)} \tilde{\phi}_f^{(2)}), \quad \tilde{\mathbf{p}} = \sum_e p_e \tilde{\phi}_e + \sum_f (p_f^{(1)} \tilde{\phi}_f^{(1)} + p_f^{(2)} \tilde{\phi}_f^{(2)}).$$

Setting

$$c_n(\tilde{\mathbf{q}}, \tilde{\mathbf{p}}) = \sum_{\text{edge } e} q_e p_e b_n(\tilde{\phi}_e, \tilde{\phi}_e) + \sum_{\text{face } f} b_n(q_f^{(1)} \tilde{\phi}_f^{(1)} + q_f^{(2)} \tilde{\phi}_f^{(2)}, p_f^{(1)} \tilde{\phi}_f^{(1)} + p_f^{(2)} \tilde{\phi}_f^{(2)}), \tag{4.12}$$

we have

$$c_1 c_n(\tilde{\mathbf{q}}, \tilde{\mathbf{q}}) \leq b_n(\tilde{\mathbf{q}}, \tilde{\mathbf{q}}) \leq c_2 c_n(\tilde{\mathbf{q}}, \tilde{\mathbf{q}}) \text{ on } \widetilde{\mathcal{ND}}_2^h$$

with c_1 and c_2 independent of the mesh size h [9]. Thus, $b_n(\cdot, \cdot)$ and $c_n(\cdot, \cdot)$ are spectrally equivalent and we can replace the error equation (4.9) by

$$c_n(\tilde{\mathbf{E}}_{n+1}^{h,loc}, \Phi) = b_n(\mathbf{A}_n - \mathbf{A}_{n+1}^{h,euler}, \Phi) + \frac{1}{\gamma} (\mathbf{R}_{n1}^h, \Phi), \quad \forall \Phi \in \widetilde{\mathcal{ND}}_2^h. \tag{4.13}$$

Let

$$\tilde{\mathbf{E}}_{n+1}^{h,loc} = \sum_e E_e \tilde{\phi}_e + \sum_f (E_{f1} \tilde{\phi}_f^{(1)} + E_{f2} \tilde{\phi}_f^{(2)})$$

be a representation of the new approximate error. Then the coefficients can be computed from small local problems, that is from a scalar equation for each edge e and a 2×2 linear equation for each face f . Using $\Phi = \tilde{\phi}_e$ in (4.13) and introducing

$$r_n(\Phi) = b_n(\mathbf{A}_n - \mathbf{A}_{n+1}^{h,euler}, \Phi) + (\mathbf{R}_{n1}^h, \Phi) / \gamma,$$

we get

$$E_e = \frac{r_n(\tilde{\Phi}_e)}{b_n(\tilde{\Phi}_e, \tilde{\Phi}_e)}. \quad (4.14)$$

Observe that $c_n(\tilde{\Phi}_f^{(i)}, \tilde{\Phi}_e) = 0$ for $i = 1, 2$. Further, $\Phi = \tilde{\Phi}_f^{(i)}$, $i = 1, 2$, yields

$$\begin{pmatrix} b_n(\tilde{\Phi}_f^{(1)}, \tilde{\Phi}_f^{(1)}) & b_n(\tilde{\Phi}_f^{(2)}, \tilde{\Phi}_f^{(1)}) \\ b_n(\tilde{\Phi}_f^{(1)}, \tilde{\Phi}_f^{(2)}) & b_n(\tilde{\Phi}_f^{(2)}, \tilde{\Phi}_f^{(2)}) \end{pmatrix} \begin{pmatrix} E_{f1} \\ E_{f2} \end{pmatrix} = \begin{pmatrix} r_n(\tilde{\Phi}_f^{(1)}) \\ r_n(\tilde{\Phi}_f^{(2)}) \end{pmatrix}. \quad (4.15)$$

Since $b_n(\tilde{\Phi}_e, \tilde{\Phi}_e) = \mathcal{O}(\varepsilon)$ with ε being the (small) regularization parameter in the non-conducting region, we simply set $E_e = 0$ there.

We conclude that the error estimator \mathbf{E}_{n+1}^h defined in (4.5) can be efficiently approximated by just a few calculations using (i) lower order in time, that is, $\mathbf{E}_{n+1}^h \approx \tilde{\mathbf{E}}_{n+1}^h$ (4.9), and (ii) localization in space, that is, $\mathbf{E}_{n+1}^h \approx \tilde{\mathbf{E}}_{n+1}^{h,loc}$ (4.13). A crucial point in the analysis of hierarchical error estimators is the saturation assumption. In its simplest form it asserts that the quadratic finite element solution in \mathcal{ND}_2^h is better than the linear solution in \mathcal{ND}_1^h . This is in general satisfied if the solution is smooth enough. However, in the case of e.g. discontinuities of the conductivity σ we get singularities and therefore lower regularity, see [9] for a more detailed discussion. More recently, a sufficient condition for the validity of the saturation assumption in terms of small data oscillation has been given in [22]. A modified saturation assumption is used in [3] to show robustness of the hierarchical estimator.

The local spatial error for a finite element $T \in \mathcal{T}_h$ can be estimated by computing the norm of $\tilde{\mathbf{E}}_{n+1}^{h,loc}$ over T . For the overall spatial error, we define in line with the local temporal error in (3.7)

$$\|\tilde{\mathbf{E}}_{n+1}^{h,loc}\| = \left(\frac{\|\tilde{\mathbf{E}}_{n+1}^{h,loc}\|_{L^2(\Omega)}^2}{ATOL + RTOL \|\mathbf{A}_{n+1}^h\|_{L^2(\Omega)}^2} \right)^{1/2}. \quad (4.16)$$

Based on this error estimation, we can control the spatial accuracy of the solution numerically computed to an imposed tolerance level TOL_x . An iterative process estimate-refine-solve within a time step is continued until $\|\tilde{\mathbf{E}}_{n+1}^{h,loc}\| < TOL_x$. Obviously, temporal and spatial errors have to be well balanced. We have also to take into account mesh coarsening to gain efficiency. Our entire control strategy will be described in the next chapter.

5. The Control Strategy

Our aim is to estimate and to control the accuracy of the solution numerically computed to the imposed tolerance levels TOL_t and TOL_x . The entire control strategy is taken from [29]. For the sake of completeness we shall give a short summary of the implementation used.

In the spirit of the adaptive Rothe method the spatial discretization is considered as a perturbation of the time integration, hence has to be controlled before estimating the temporal error. Suppose we are given an approximate solution \mathbf{A}_{n-1}^h on the finest, already accepted mesh \mathcal{T}_{n-1} at time t_{n-1} . Applying the estimation process described in the previous chapter and grid refinement afterwards, we construct a sequence of improved spatial meshes for the new solution \mathbf{A}_n^h

$$\mathcal{T}_n^0 \subset \mathcal{T}_n^1 \subset \dots \subset \mathcal{T}_n^{m_n}, \quad (5.1)$$

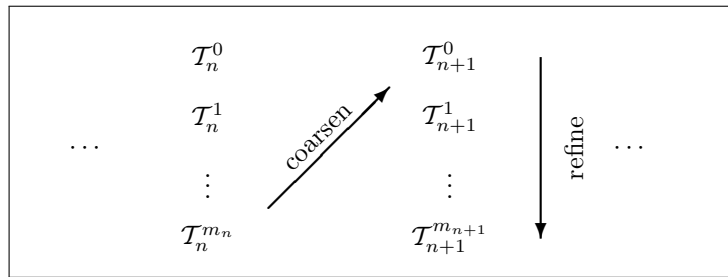


Fig. 5.1. Refinement and coarsening. A sequence of improved spatial meshes $\mathcal{T}_n^0 \subset \mathcal{T}_n^1 \subset \dots \subset \mathcal{T}_n^{m_n}$ is constructed until TOL_x is reached at level m_n . If the time step is accepted, a new initial mesh \mathcal{T}_{n+1}^0 is constructed through removing elements with sufficiently small error estimators. Then the process of estimate and refine starts again.

which also generates a nested sequence of $\mathbf{H}_0(\mathbf{curl})$ -conforming FE-spaces. Note that we do not use coarsening here. The refinement process (5.1) is guided by the local quantities $\eta_T = \|\tilde{\mathbf{E}}_n^{i,loc}\|_{T}, T \in \mathcal{T}_n^i$, that is the a posteriori error estimator for the finite element T at refinement level i . New grid points should be placed in regions of insufficient accuracy. Therefore all elements with $\eta_T > 0.8 \max_T \eta_T =: \eta_{bar}$ are refined. We use the regular red-green refinement strategy for tetrahedral elements (see e.g. [29] and references therein). The multilevel process is stopped if for a certain number m_n the approximate global error $\|\tilde{\mathbf{E}}_n^{m_n,loc}\|$ is less than TOL_x .

After successful improvement of the spatial grid the local temporal error is estimated on the finest grid by r_n defined in (3.7). If $r_n \geq TOL_t$ the step is not accepted and redone with a reduced value of τ_n determined from (3.8). Additionally, all meshes $\mathcal{T}_n^i, i > 0$ are also removed. If $r_n < TOL_t$ we set $\mathcal{T}_n = \mathcal{T}_n^{m_n}$ and advance in time with the new initial solution \mathbf{A}_n^h computed on \mathcal{T}_n . It remains to choose an initial mesh at t_{n+1} , see Fig. 5.1.

Clearly, the mesh \mathcal{T}_{n+1}^0 should be an approximation of the final mesh \mathcal{T}_n obtained in the previous step. To be efficient, elements have to be removed in regions of small errors. They can be detected by their η -values. Assuming an asymptotic behaviour $\eta \sim ch^2$ for the weighted L^2 -norm, a prediction of the η -values after coarsening will be $\eta_{predict} \sim 4\eta$. We remove an element $T \in \mathcal{T}_n$ if the predicted value does not exceed the local error barrier η_{bar} . One point ought to be mentioned: Modern adaptive codes which allow refinement and coarsening employ sophisticated tree structures based on so-called father-son relations. Usually, elements (the sons) that were obtained from refining a coarser element (the father) can be removed only simultaneously.

In Fig. 5.2 we show a flow chart for the entire space-time coupled adaptive approach as implemented in the KARDOS software package [2]. First, in an inner loop the spatial accuracy is controlled. Then the temporal error is checked and it is decided whether the time step is accepted.

6. Numerical Results

To demonstrate the performance of the local error estimators and the control strategy, we consider the magnetic recording write head problem [24]. We set $ATOL=0.01$ and $RTOL=1.0$ in (3.7) and (4.16) for an appropriate error control. The results are computed with the PDE-software package KARDOS [2] and are visualized with AMIRA [1].

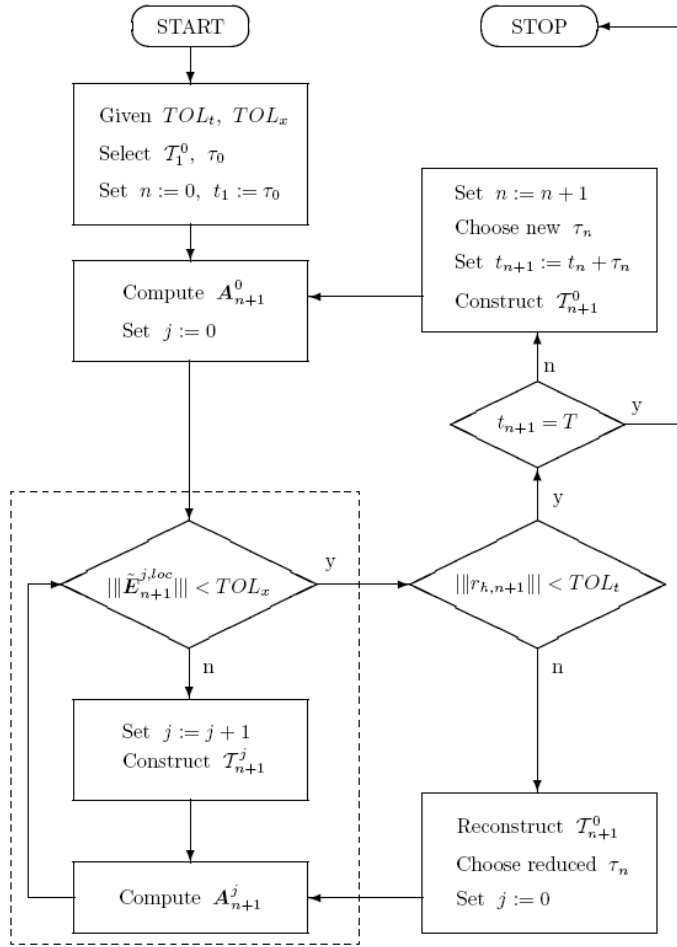


Fig. 5.2. Flow chart for the time-space adaptive solver KARDOS. First, approximate solutions \mathbf{A}_{n+1}^j to $\mathbf{A}(x, t_{n+1})$ are computed on a sequence of triangulations $\mathcal{T}_{n+1}^0 \subset \mathcal{T}_{n+1}^1 \subset \dots \subset \mathcal{T}_{n+1}^j$ until TOL_x is reached. Then the local error in time $\|r_{h,n+1}\|$ is checked. If it is smaller than TOL_t the step is accepted and we advance in time. Otherwise, the step is rejected and redone. In this case all refinements made are removed and the original initial mesh \mathcal{T}_{n+1}^0 is reconstructed.

The thin film magnetic recording write head problem has been proposed by the Storage Research Consortium (SRC) in Japan as a benchmark for computational electro-magnetics. A detailed description of the nonlinear transient eddy current benchmark model for a 2 Gb/in² harddisc read write head design is given in [24]. The applied magnetomotive force (mmf) is a part of trapezoidal waveform of 25 MHz including higher harmonics, Fig. 6.1(a). Even though switching times for the exciting currents range in the nanosecond region (qualifying the device as a high frequency device), a careful frequency analysis shows the validity of the magnetoquasistatic assumptions [14]. The yoke material is permalloy having a conductivity $\sigma = 5 \times 10^6$ S/m and a magnetic permeability modelled by the B-H curve in Fig. 6.1(b).

Extensive numerical simulations employing uniform temporal and spatial discretizations have been performed to verify the vertical magnetic flux $B_z(t)$ near the pole tip of the magnetic head, which could be measured by a stroboscopic electron beam tomography [24]. Good

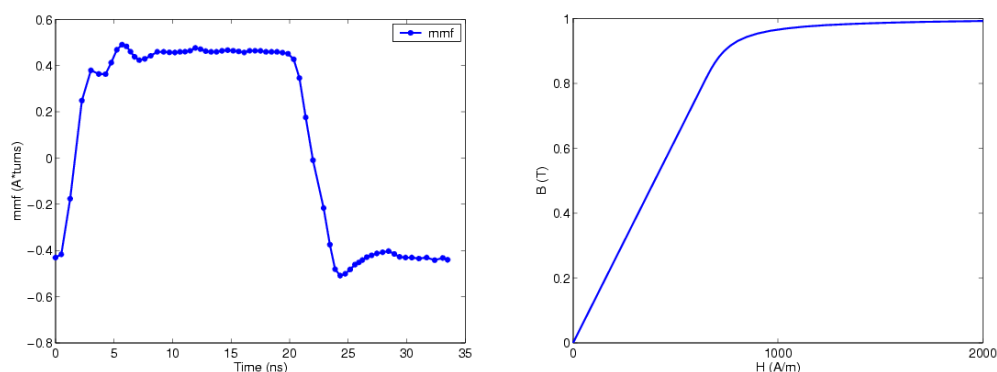


Fig. 6.1. (a) The applied magnetomotive force (mmf) taken from [24]. (b) B-H curve of the permalloy material with initial relative permeability $\mu_s = 1000$ and saturation magnetization $M_s = 1$ T.

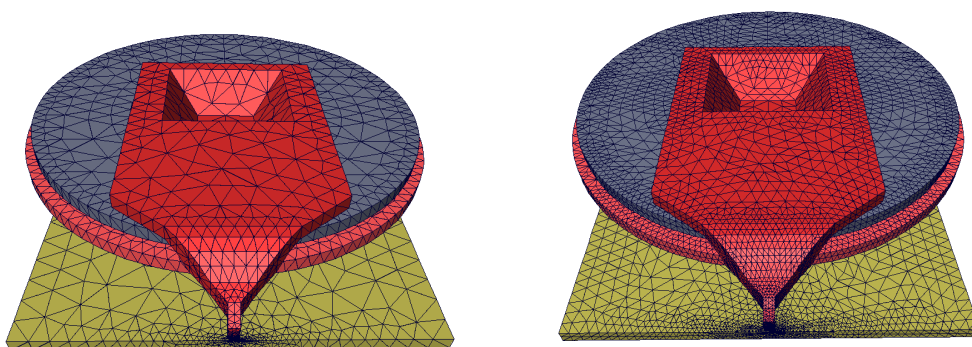


Fig. 6.2. (a) Tetrahedral mesh used for the initial discretization of the write head geometry consisting of permalloy yoke, upper and lower copper coil, and permalloy plate (16 708 nodes). The device length is $148 \mu\text{m}$. The seven upper and eight lower coil strands are lumped to two single coils. (b) A typical adapted mesh created by the refinement approach proposed (56 472 nodes). The surrounding mesh for the air region is not shown.

agreement is achieved if the numerically calculated B_z -curve reflects accurately the dynamic behaviour of the applied magnetomotive force. In Fig. 6.3, we present results for time adaptive runs using two Rosenbrock methods, the two-stage second-order ROS2 [20, 29] and the newly designed four-stage third-order ROS3PL. We use the coarse grid shown in Fig. 6.2(a), set $TOL_t = 2 \times 10^{-5}$ and start all computations with the initial step $\tau_0 = 5 \times 10^{-8}$. The results are compared with a fully space-time adaptive ROS3PL-run, where we also apply mesh adaptation to reach the local spatial tolerance $TOL_x = 1.0 \times 10^{-5}$. It can be nicely seen that the quality of solution delivered by the fully adaptive ROS3PL is quite satisfactory, especially in regions of fast increase and decrease of the applied magnetomotive force. Moreover, an improved spatial mesh leads also to a drastic reduction of the number of variable time steps chosen by ROS3PL to keep the local temporal error below the imposed tolerance TOL_t . Without spatial adaptation we count 156 steps, while only 67 steps are required when automatic mesh improvement is considered.

In Fig. 6.4 we depict the evolution of time steps and degrees of freedom (dofs) for the time-space adaptive simulation. The time steps lie between 3.1×10^{-10} and 1.0×10^{-9} , seven steps are rejected. At the beginning the initial spatial mesh having 109 495 dofs is rapidly refined to

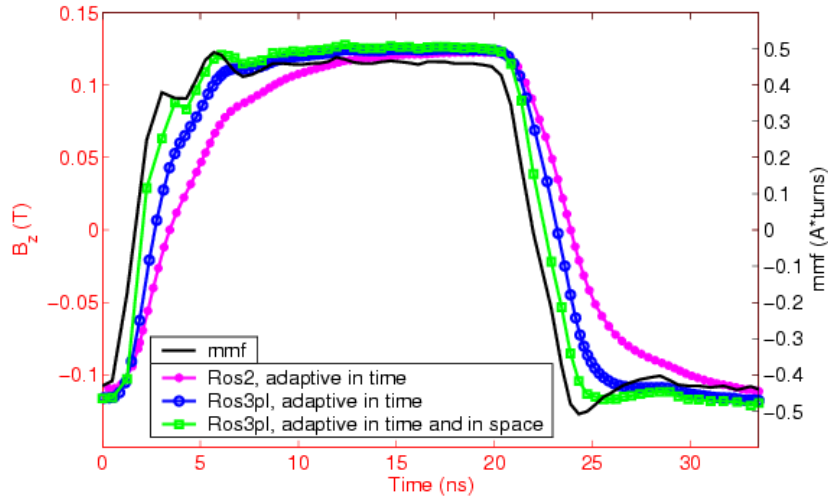


Fig. 6.3. Comparison of $B_z(t)$ computed near the pole tip of the magnetic head with the two-stage second-order ROS2 method [20] and the newly designed four-stage third-order ROS3PL. Notably good agreement is achieved for the fully time-space adaptive ROS3PL, especially in regions of fast increase and decrease of the applied magnetomotive force.

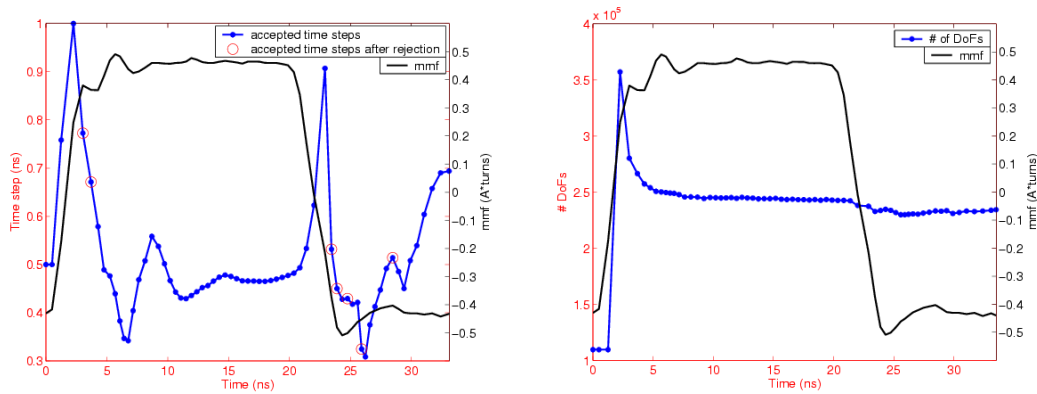


Fig. 6.4. Evolution of variable time steps and degrees of freedom chosen by the fully adaptive ROS3PL to reach $TOL_t = 2.0 \times 10^{-5}$ and $TOL_x = 1.0 \times 10^{-5}$.

357 173 dofs to reflect the solution's dynamics properly. Later on, after successive coarsening, around 250 000 dofs are quite efficient. The maximum refinement depth equals three. That means, a comparable uniform approach would be forced to use approximately 56 mio. dofs, wasting tremendous resources of computing time.

7. Conclusion

We have combined variable step size one-step methods of Rosenbrock type and adaptive $\mathbf{H}(\mathbf{curl})$ -conforming Whitney finite elements to solve nonlinear three-dimensional magnetoquasistatics problems. On the basis of numerical investigations for the thin film magnetic recording write head problem and the TEAM7 benchmark problem already discussed in [31] we have come to the following conclusions. (i) Automatic control of discretization errors is quite

attractive from a practical point of view. Time consuming validation of numerical solutions usually done through parameter tuning in repeated calculations is no longer needed. (ii) Well designed linearly implicit Rosenbrock methods as e.g. ROS3PL work remarkably reliable. Although they are nearly as simple as explicit integrators (only an appropriate Jacobian has to be provided), they are unconditionally stable with excellent stability properties for systems of differential-algebraic equations. Moreover, one-step methods allow fast step size changes and the handling of well fitted individual spatial meshes at different time points without any specific difficulties. (iii) Hierarchical error estimators based on approximate dynamics and suitable spatial surplus spaces give efficient and reliable estimates for local error distributions. Taking into account interpolation errors and error transport over the entire time interval is essential. Finally, well-balanced dynamic spatial meshes can improve the performance of the time integrator significantly.

8. Appendix

We give the set of coefficients for ROS3PL with double-precision accuracy.

Table. A1: Set of coefficients for ROS3PL - a third-order accurate Rosenbrock method constructed along the design criteria: (i) L-stable and stiffly accurate, (ii) no order reduction when applied to parabolic PDEs, and (iii) third-order accurate W-method for Jacobians perturbed by $\mathcal{O}(\tau)$ -terms.

$\gamma = 4.358665215084590e - 01$	
$a_{11} = 0.000000000000000e + 00$ $a_{21} = 1.147140180139521e + 00$ $a_{22} = 0.000000000000000e + 00$ $a_{31} = 2.463070773030053e + 00$ $a_{32} = 1.147140180139521e + 00$ $a_{33} = 0.000000000000000e + 00$ $a_{41} = 2.463070773030053e + 00$ $a_{42} = 1.147140180139521e + 00$ $a_{43} = 0.000000000000000e + 00$ $a_{44} = 0.000000000000000e + 00$	$\alpha_1 = 0.000000000000000e + 00$ $\alpha_2 = 5.000000000000000e - 01$ $\alpha_3 = 1.000000000000000e + 00$ $\alpha_4 = 1.000000000000000e + 00$
$c_{11} = 2.294280360279042e + 00$ $c_{21} = 2.631861185781065e + 00$ $c_{22} = 2.294280360279042e + 00$ $c_{31} = 1.302364158113095e + 00$ $c_{32} = -2.769432022251304e + 00$ $c_{33} = 2.294280360279042e + 00$ $c_{41} = 1.552568958732400e + 00$ $c_{42} = -2.587743501215153e + 00$ $c_{43} = 1.416993298352020e + 00$ $c_{44} = 2.294280360279042e + 00$	$s_{11} = 0.000000000000000e + 00$ $s_{21} = 2.631861185781065e + 00$ $s_{22} = 0.000000000000000e + 00$ $s_{31} = 5.650974900540168e + 00$ $s_{32} = 2.631861185781065e + 00$ $s_{33} = 0.000000000000000e + 00$ $s_{41} = 5.650974900540168e + 00$ $s_{42} = 2.631861185781065e + 00$ $s_{43} = 0.000000000000000e + 00$ $s_{44} = 0.000000000000000e + 00$
$\gamma_1 = 4.358665215084590e - 01$ $\gamma_2 = -6.413347849154100e - 02$ $\gamma_3 = 1.110281725125051e - 01$ $\gamma_4 = 0.000000000000000e - 00$	$d_1 = 0.000000000000000e + 00$ $d_2 = 1.147140180139521e + 00$ $d_3 = 2.294280360279042e + 00$ $d_4 = 2.294280360279042e + 00$
$m_1 = 2.463070773030053e + 00$ $m_2 = 1.147140180139521e + 00$ $m_3 = 0.000000000000000e + 00$ $m_4 = 1.000000000000000e + 00$	$\hat{m}_1 = 2.346947683513665e + 00$ $\hat{m}_2 = 4.565305694518951e - 01$ $\hat{m}_3 = 5.694924394549457e - 02$ $\hat{m}_4 = 7.386849361662244e - 01$

Acknowledgment. This work is partly supported by the Deutsche Forschungsgemeinschaft (DFG) within the project “Space-time adaptive magnetic field computation” (grants CL143/3-1, CL143/3-2, LA1372/3-1, LA1372/3-2).

References

- [1] <http://amira.zib.de/>
- [2] <http://www.zib.de/Numerik/software/kardos>
- [3] B. Achchab, S. Achchab, A. Agouzal, Some remarks about the hierarchical a posteriori error estimate, *Numer. Math. for PDEs*, **20** (2004), 919-932.
- [4] M. Ainsworth, J. Coyle, Hierarchic finite element basis on unstructured tetrahedral meshes, *Int. J. Numer. Meth. Eng.*, **58**:14 (2003), 2103-2130.
- [5] F. Bachinger, U. Langer, J. Schöberl, Numerical analysis of nonlinear multiharmonic eddy current problems, *Numer. Math.*, **100** (2005), 593-616.
- [6] F. Bachinger, U. Langer, J. Schöberl, Efficient solvers for nonlinear time-periodic eddy current problems, *Comp. Vis. Sci.*, **9** (2006), 197-207.
- [7] R. Beck, P. Deuffhard, R. Hiptmair, R.H.W. Hoppe, B. Wohlmuth, Adaptive Multilevel Method for Edge Element Discretizations of Maxwell’s Equations, *Surveys on Math. for Industry*, **8** (1998), 271-312.
- [8] R. Beck, R. Hiptmair, R. Hoppe, B. Wohlmuth, Residual based a posteriori error estimators for eddy current computations, *M²AN*, **34** (2000), 159-182.
- [9] R. Beck, R. Hiptmair, B. Wohlmuth, Hierarchical error estimator for eddy current computation, Proc. ENUMATH 99, P. Neittaanmäki et al. (eds.), 110-120, World Scientific, Singapore, 1999.
- [10] R. Becker, R. Rannacher, An optimal control approach to a posteriori error estimation in finite element methods, *Acta numerica*, **10** (2001), 1-102.
- [11] P. Bochev, C. Garasi, J. Hu, A. Robinson, R. Tuminaro, An improved algebraic multigrid method for solving Maxwell’s equations, *SIAM J. Sci. Comput.*, **25** (2003), 623-642.
- [12] D. Braess, J. Schöberl, Equilibrated residual error estimators for Maxwell’s equations, *Math. Comput.*, **77** (2008), 651-672.
- [13] F. Cameron, R. Piché, K. Forsman, Variable step size time integration methods for transient eddy current problems, *IEEE T. Magn.*, **34**:5 (1998), 3319-3323.
- [14] M. Clemens, S. Drobny, T. Weiland, Numerical analysis of a magnetic recording write head benchmark problem using the finite integration technique, *IEEE T. Magn.*, **38** (2002), 601-604.
- [15] M. Clemens, M. Wilke, and T. Weiland, 3D transient eddy current simulations using FI²TD with variable time step size selection schemes, *IEEE T. Magn.*, **38**:2 (2002), 605-608.
- [16] M. Clemens, M. Wilke, T. Weiland, Linear-implicit time integration schemes for error-controlled transient nonlinear magnetic field simulations, *IEEE T. Magn.*, **39** (2003), 1175-1178.
- [17] M. Clemens, S. Feigh, T. Weiland, Geometric Multigrid Algorithms Using the Conformal Finite Integration Technique, *IEEE T. Magn.*, **40**:2 (2004), 1065-1068.
- [18] M. Clemens, Large systems of equations in a discrete electromagnetism: formulations and numerical algorithms, *IEE P. - Sci., Meas Tech.*, **152**:2 (2005), 50-72.
- [19] M. Clemens, S. Feigh, T. Weiland, Construction principles of multigrid smoothers for curl-curl equations, *IEEE T. Magn.*, **41**:5 (2005), 1680-1683.
- [20] K. Dekker, J. Verwer, Stability of Runge-Kutta Methods for Stiff Nonlinear Differential Equations, North-Holland, Elsevier Science Publishers, 1984.
- [21] P. Deuffhard, P. Leinen, H. Yserentant, Concepts of an adaptive hierarchical finite element code, *IMPACT Comp. Sci. Engrg.*, **1** (1989), 3-35.
- [22] W. Dörfler, R.H. Nochetto, Small data oscillation implies saturation assumption, *Numer. Math.*, **91** (2002), 1-12.

- [23] B. Erdmann, J. Lang, R. Roitzsch, KARDOS User's Guide, Technical Report ZR-02-42, ZIB, 2002.
- [24] K. Fujiwara, F. Ikeda, A. Kameari, Y. Kanai, K. Nakamura, N. Takahashi, K. Tani, and T. Yamada, Thin film write head field analysis using a benchmark problem, *IEEE T. Magn.*, **36** (2000), 1784-1788.
- [25] K. Gustafsson, M. Lundh, G. Söderlind, A PI stepsize control for the numerical solution of ordinary differential equations, *BIT*, **28** (1988), 270-287.
- [26] E. Hairer, G. Wanner, Solving Ordinary Differential Equations II, Stiff and Differential-Algebraic Equations, Second Revised Edition, Springer-Verlag, 1996.
- [27] M. Heroux, R. Bartlett et al., An Overview of Trilinos, Sandia National Laboratories, Technical Report SAND2003-2927, 2003.
- [28] R. Hiptmair, Multigrid method for Maxwell's equations, *SIAM J. Numer. Anal.*, **36**:1 (1999), 204-225.
- [29] J. Lang, Adaptive Multilevel Solution of Nonlinear Parabolic PDE Systems. Theory, Algorithm, and Applications, LNCSE vol. 16, Springer-Verlag, 2000.
- [30] J. Lang, J. Verwer, ROS3P - an accurate third-order Rosenbrock solver designed for parabolic problems, *BIT*, **41** (2001), 730-737.
- [31] J. Lang, D. Teleaga, Towards a fully space-time adaptive FEM for magnetoquasistatics, *IEEE T. Magn.*, **44** (2008), 1238-1241.
- [32] P. Monk, A posteriori error indicators for Maxwell's equations, *J. Comput. Appl. Math.*, **100** (1998), 173-190.
- [33] J. Nédélec, Mixed finite elements in R^3 , *Numer. Math.*, **35** (1980), 315-341.
- [34] S. Reitzinger, J. Schöberl, An algebraic multigrid method for finite element discretizations with edge elements, *Numer. Linear. Algebr.*, **9** (2002), 223-23.
- [35] S. Reitzinger, B. Kaltenbacher, M. Kaltenbacher, A Note on the Approximation of B-H Curves for Nonlinear Magnetic Field Computations, SFB-Report 02-30, Johannes-Kepler-University Linz, SFB Numerical and Symbolic Scientific Computing, 2002.
- [36] Z. Ren, Influence of R.H.S. on the convergence behaviour of the curl-curl equation, *IEEE T. Magn.*, **12** (1996), 655-658.
- [37] J. Schöberl, A posteriori error estimates for Maxwell equations, *Math. Comput.*, **77** (2008), 633-649.
- [38] O. Sterz, A. Hauser, G. Wittum, Adaptive local multigrid methods for solving time-harmonic eddy-current problems, *IEEE T. Magn.*, **42** (2006), 309-318.
- [39] A. Vande Wouwer, Ph. Saucez, W.E. Schiesser (eds.), Adaptive Methods of Lines, Chapman& Hall/CRC 2001.
- [40] H. Wang, S. Taylor, J. Simkin, C. Biddlecombe, B. Trowbridge, An adaptive-step time integration method applied to transient magnetic field problems, *IEEE T. Magn.*, **37**:5 (2001), 3478-3481.
- [41] G. Wimmer, T. Steinmetz, M. Clemens, Error control schemes for adaptive time integration of magnetodynamic systems with variable spatial mesh resolution, *COMPEL*, **26**:3 (2007), 758-772.
- [42] W. Zheng, Z. Chen, L. Wang, An adaptive finite element method for the h - ψ formulation of time-dependent eddy current problems, *Numer. Math.*, **103** (2006), 667-689.